Lawrence Berkeley National Laboratory

Lawrence Berkeley National Laboratory

Title
Measurement of the indium segregation in InGaN based LEDs with single atom sensitivity

Permalink
https://escholarship.org/uc/item/9444p5jb

Authors
Jinschek, Joerg
Kisielowski, Christian
Van Dyck, Dirk
et al.

Publication Date
2003-07-30

eScholarship.org Powered by the California Digital Library
University of California

Measurement of the indium segregation in InGaN based LEDs with single atom sensitivity

Joerg R. Jinschek[*a], Christian Kisielowski [a], Dirk Van Dyck [b], Philippe Geuens [b]
[a] National Center for Electron Microscopy (NCEM), Lawrence Berkeley National Laboratory (LBNL), University of California, One Cyclotron Road MS R720150, Berkeley/CA, USA 94720;
[b] EMAT, University of Antwerp, Groenenborgerlaan 171, B-2020 Antwerp, Belgium

ABSTRACT

In light emitting diodes (LED) consisting of GaN / InGaN / GaN quantum wells (QWs), the exact indium distribution inside the wells of the active region affects the performance of devices. Indium segregation can take place forming small InGaN clusters of locally varying composition. In the past, we used a local strain analysis from single HRTEM lattice images to determine the In composition inside the InGaN QWs with a resolution of 0.5 nm x 0.3 nm. Truly atomic resolution can be pursued by exploitation of intensity dependencies on the atomic number (Z) of the electron exit-wave (EW). In microscopes with sufficient sensitivity, local variations of amplitude and phase are found to be discrete with sample thickness, which allows for counting the number of atoms in each individual column of ~ 0.08 nm diameter. In QW's of ~ 17% of average indium concentration it is possible to discriminate between pure Ga columns and columns containing 1, 2, 3, or more In atoms because phase changes are discrete and element specific. The preparation of samples with atomically flat surfaces is a limiting factor for the application of the procedure.
Keywords: indium gallium nitride (InGaN), gallium nitride (GaN), quantum well, indium (In) distribution / segregation, transmission electron microscopy, HRTEM, phase contrast, exit wave reconstruction (EWR)

1. INTRODUCTION

In recent years, gallium nitride (GaN) and its alloys (aluminum gallium nitride - AlGaN or indium gallium nitride - InGaN) have attracted special interest since the high brightness green, blue, and white light emitting diodes (LED's) became commercially available for solid state lighting [1]. Green and blue LED devices contain in the active region few Ångstrom (1Å = 10^{-10}m) wide InGaN QW's sandwiched between a p- and a n-doped GaN matrix. The distribution of indium atoms in such wells can affect the device performance. A number of reports have shown that indium clustering takes places in InGaN QWs with 10-30% of In concentration [2, 3]. Indium concentrations around 45% for green light emission were experimentally never observed [4].
Quantitative measurements of the local indium concentration require high resolution transmission electron microscopy (HRTEM) studies or high annular angle dark field (HAADF) scanning transmission electron microscopy (STEM) investigations [5]. Progress with HRTEM enables the reconstruction of the electron exit waves (EWR) by holographic recording techniques from focal series of lattice images [6] (or from a single off-axis electron hologram [7]). Unlike lattice images which are beam interferrograms, both HAADF imaging and EWR can provide direct images of the crystal structure.
In the past the measurement of lattice parameters from single HRTEM lattice images [2] was used to determine displacement fields and strain from which the local indium composition in the QWs can be derived with a resolution of 0.5 x 0.3 nm^2. In this paper we determine the atomic In distribution from the amplitude and phase of EW images. We benefit from a resolution extension to sub Ångstrom values [8] and from a high sensitivity of the One Ångstrom Microscope (OAM) at NCEM that is aberration corrected to third order. Since the generated amplitude and phase values of the EW depend on the atomic number Z it possible to discriminate between gallium and indium atoms within one column at a well defined sample thickness. We use multi-slice calculations along with simulated EW images to test and discuss sensitivity, limits, and error bars. Using the comparison between simulations and experiment we find that our sensitivity suffices to detect one single indium atom in a column of gallium atoms inside the InGaN QW. Results

[*] JRJinschek@lbl.gov; phone +1 510 486.4590; fax +1 510 486.5888; http://ncem.lbl.gov

obtained from strain mapping provide an intrinsic check of the methods validity that can be applied to any crystalline materials system.
A major bottleneck affecting the success of quantitative measurements is the sample preparation to electron transparency for HRTEM (sample thickness < 10 nm). There are different approaches to prepare high quality samples such as a final low angle, low voltage argon (Ar^+) ion milling process after conventional mechanical dimpling [8], the tripod polishing method showing promising results for oxides and ceramics [9], or chemical etching after ion milling [2]. In this paper we establish the use of a focused ion beam (FIB) together with a wet etching process for the preparation of high quality GaN samples. The FIB method exhibits several advantages: it allows sample preparation from very small sample volumes, shows almost no preferential etching, and allows site-specific preparation. This makes this method very suitable for device characterization and failure analysis by TEM [10].

2. METHODOLOGY

2.1 Reconstruction of the complex object exit wave function (EWR)

Today, processing of lattice images allows recovering the complex electron exit wave (EW) from a focal series of images using the FEI program package "TrueImage" that bases on the PAM/MAL algorithm by Coene and Thust [11,12]. All focal series were taken with the OAM, a CM300 FEG/UT microscope. It exhibits a uniquely large signal to noise (S/N) ratio for the detection of phase changes that was tested with a gold sample [13]. Its ability to detect small signals was demonstrated by imaging light atom columns made from nitrogen in GaN, oxygen in sapphire, or carbon in diamond [8]. In the holographic reconstruction process the defocus dependence of lattice image patterns is eliminated and delocalization as well as lens aberrations up to the 3rd order can largely be reduced [14]. A direct image of the crystal structure can be obtained with minimal distortions. Further, the procedure extends the resolution of microscope up to its information limit that can reach sub Ångstrom values of ~0.8Å [8,15].

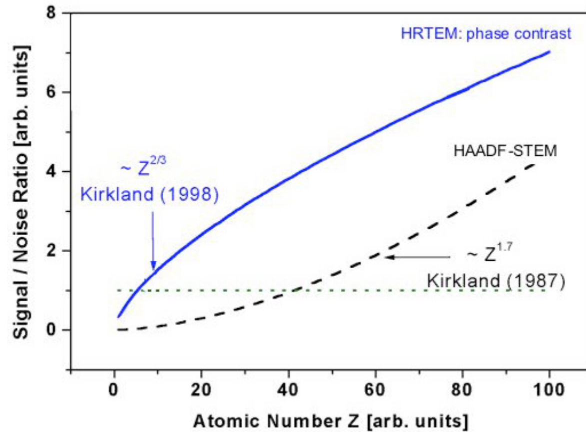

Figure 1: Sensitivity of HRTEM phase imaging (EW reconstruction, $\sim Z^{2/3}$), and HAADF-STEM imaging ($\sim Z^{1.7}$) for the detection of single atoms with atomic number. For gold our measured signal to noise (S/N) ratio is 5-6 (phase change of 0.53 rad per atom with 0.1 rad noise) A S/N ratio of 1 is considered to be the detection limit.

Unlike phase contrast imaging, incoherently scattered electrons are recorded on a ring detector in HAADF-STEM that produces direct crystal structure images without additional processing. The signal can increase almost quadratically with the atomic number Z giving the method the name "Z-contrast imaging" [16,17]. Watanabe et al. [5] have used this method to measure In content in InGaN QWs with limited success due to noise problems. Figure 1 shows an estimate of sensitivity for HAADF-STEM and EWR, which can be utilized to understand and design experiments that aim for single atom detection [18]. It was generated measuring the signal to noise (S/N) ratio for the detection of a single gold atom by HAADF-STEM and EWR and utilizing theory for the extrapolation across elements of the Periodic Table. A S/N ratio of 1 is considered the detection limit. Phase contrast microscopy generally has a better S/N ratio for the detection of single atoms, and one can anticipate that even individual light atoms can be distinguished (Z > 5-10). Z-contrast microscopy allows for better discrimination between different elements because of the concave character (amplification) of the signal dependence on Z. Single atom sensitivity is obtained for elements with Z larger than about 40. For example, P. M. Voyles et al. [19,20] recently reported the detection of single antimony (Sb, Z = 51) atoms in silicon (Z = 14) by HAADF-

STEM imaging. This experiment could only be performed because of the appreciable Z difference of these elements ($\Delta Z = 37$). Single Sb atoms can be detected but single silicon atoms not (see noise level in Fig. 1).

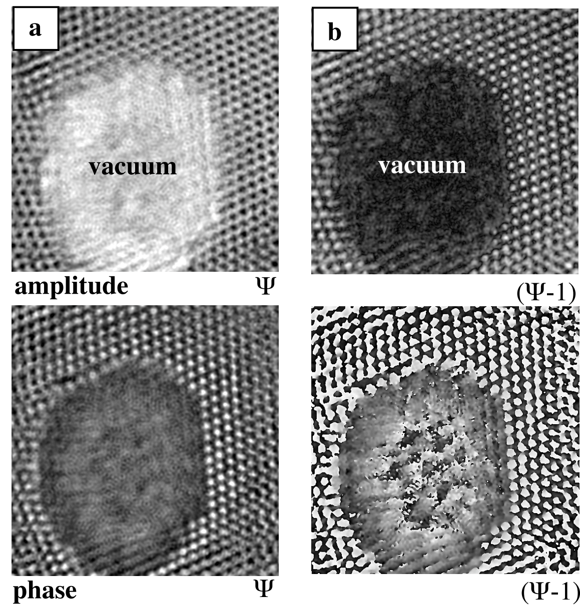

Figure 2: Gold [110] (a) Amplitude and phase image of reconstructed exit wave (EW) Ψ; (b) amplitude and phase image of Ψs = Ψ-1 = (Ψ-Ψν) / Ψν .

Our new method was tested on samples of gold. This material is exceptionally suitable for measuring the S/N ratios because of its large electron scattering power (large Z = 79) and the fact that samples can be prepared without any amorphous surface layers that mostly covers sample surfaces as a result of ion milling or oxidation [21]. Such layers reduce S/N ratios substantially. Figure 2a (top and bottom) shows the reconstructed amplitude and phase of the electron exit wave Ψ from a wedge of gold as produced by the TrueImage software.

The channeling theory [22] and the related S-state model [23] describe the dynamical scattering of electrons in thin specimen in zone-axis orientation in a simple and intuitive way, thereby providing better transparency. It suggests retrieving a more direct interpretable electron wave function, namely the channeling wave Ψs, that is trapped at atomic columns instead of analyzing the total electron wave Ψ as calculated and shown in Fig. 2a. Ψs relates to Ψ by Ψs = (Ψ-Ψν) / Ψν where Ψν is the entrance (vacuum) wave. Figure 2b shows the amplitude and phase images of Ψs to be compared with Fig. 2a. Several predictions of the S-state model are verified: the amplitude of Ψs is strongly peaked at the atom column positions while the phase is constant and proportional to the column "weight" which is determined by the chemical nature of the atoms and their spacing along the column direction parallel to the electron beam. The amplitude of Ψs oscillates periodically (sinus) as function of thickness and the phase increases linearly with thickness with a phase change per atom that is characteristic for the considered element [24].

Extracting amplitude and phase at the column position from Ψs (Fig. 2b) and plotting it in an Argand diagram produces Fig. 3a (bottom) that can be verified by multi-slice calculations in Fig. 3a (top). The discrete nature of the plot directly reveals that each atomic column is build from a distinguishable number of gold atoms. Sample thickness increases atom by atom along a counter clockwise rotation along the circle. However, the complex multi-slice calculations tend to mask the physical background of the underlying scattering processes and a more intuitive description can be obtained by data reduction to the framework of the channeling theory [24].

It should be noted that Sinkler and Marks [25] produced similar plots earlier but did not succeed in revealing the entire functional dependencies. We choose to refer to this description as a channeling map [24]. Again, its validity can be confirmed by multi-slice calculations (Fig. 3a (top), Ψs plot from multi-slice calculations; simulated gold [110] wedge shaped sample with 10 atomic steps, 300 keV, debye waller = 0.5 $Å^{-2}$). The full circle of the experimental channeling map consists of 12 data points each corresponding to one extra Au atom in the column. The phase change at a single gold atom is 2 pi/12 = 0.53 rad (see angular distribution in Fig. 3b). Fitting Gaussians to the peaks of Fig. 3b, we extract a

noise level of 0.1 rad (1 sigma) and a resulting S/N ratio between 5 and 6 for the detection of a single gold atom in case of EWR. This S/N value agrees with the data published before [13].

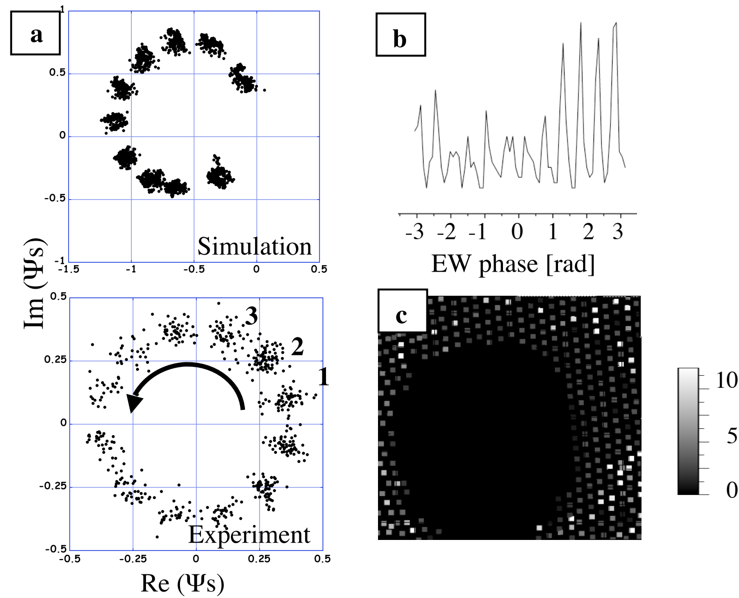

Figure 3: (a) Channeling map (Argand plot) - top - of a multi slice simulated gold wedge (with 10 atomic steps) and - bottom - of the measured EW amplitude and phase values from Fig. 2b; (b) angular distribution of the experimental data in (a); (c) recreated thickness map (3D) using the EW values from Fig. 2b and the discrete phase change per single gold atom in (a) [24,26]

Further, the channeling map allows determining the height (thickness) of each column with single atom sensitivity and a 3-dimensional (3D) thickness map (Fig. 3c) can be obtained.
Our current effort concentrates on an extension of this method to systems of different chemical elements and to columns with mixed chemical composition. Next, we use this approach to differentiate single indium - from gallium atoms in mixed $In_XGa_{(1-X)}$ atom columns ($Z_{Ga} = 31$, $Z_{In} = 49$, $\Delta Z = 18$).

3. DATA

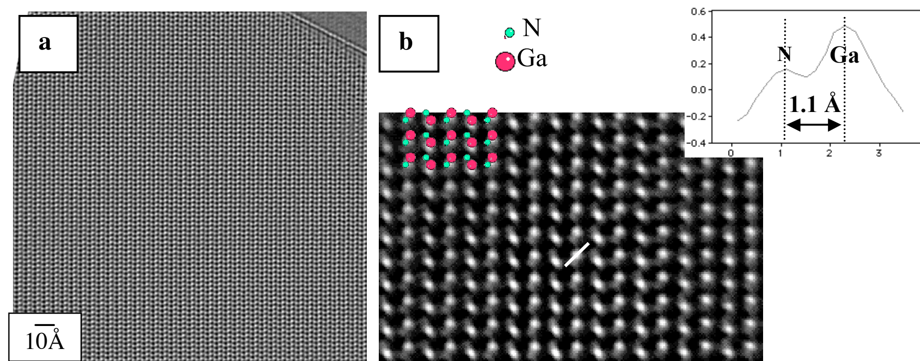

Figure 4: Reconstructed EW (Ψ) phase images in [11$\bar{2}$0] zone axis orientation ((b) with higher magnification than (a)) of the GaN matrix after FIB specimen preparation with subsequential KOH etching procedure. The in (b) inserted structure model and the line scan show the separation of the Ga and the N atomic column (1.12Å).

3.1 TEM sample preparation by Focused Ion Beam (FIB)

MOCVD grown GaN samples containing InGaN QWs were prepared for [11$\bar{2}$0] cross section observation by producing thin membranes from selected sites in a FIB process. One sample is a green LED investigated some time ago [4] the other

one was recently grown. First a rough cutting with Ga ion accelerated by 30 keV was applied followed by a cleaning procedure at 10 keV [27] that reduces the amorphous layer thickness. Thereafter, the sample was removed from the FIB and a wet KOH etch was used for stripping the FIB induced side-wall damage and the Ga implant (details [28]). Figure 4 shows a phase image of a reconstructed electron exit wave from a sample prepared in this manner. Only a very thin amorphous layer is present. Further, the chemical etching produced atomically flat crystal surfaces. They are desirable to avoid confusion between chemical- and thickness changes as will be discussed later. Ga and the N columns can be imaged and separated in [11$\underline{2}$0] orientation where the columns are only 1.13 Å apart (see line scan in Fig. 4b).

3.2 Strain analyses by HRTEM images

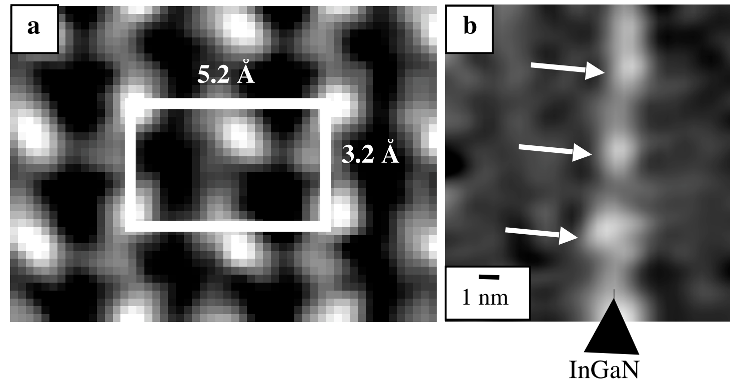

Figure 5: (a) EW image showing a single unit cell of (In)GaN in [11$\underline{2}$0] projection of ~ 0.5 x 0.3 nm^2 as the smallest unit (resolution) of the strain analyses; (b) scaled displacement field of an InGaN QW mapping the local indium concentration (arrows: high In concentration inside an inhomogeneous distribution)

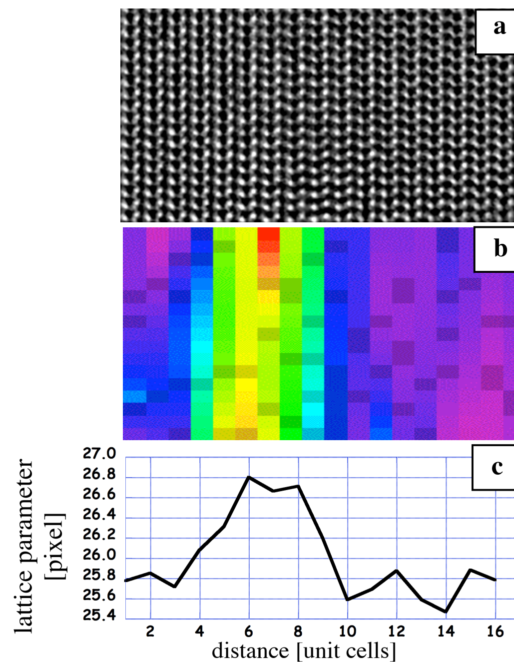

Figure 6: (a) Reconstructed EW image of an InGaN QW at larger magnification; (b) c-axis strain map and (c) averaged strain profile across the well.

Maps of the local indium concentration were produced by analyses of strain [2]. In this approach a calibrated lattice expansion due to an incorporation of indium atoms is exploited that increases the local diameter of the InGaN c-axis of the projected unit cell that is shown in Fig. 5a. Figure 5b shows the resulting displacement field of a single InGaN QW in a green LED (for further details see [4]. The displacement field can be scaled and used for mapping of local indium concentration. The presence of an inhomogeneous In distribution is evident (see arrows). The determined averaged In content is 21.0±1.2% with an In (strain) fluctuation of about 6%.
Figure 6a depicts a reconstructed electron exit wave of our recent InGaN / GaN sample at larger magnification together with a strain map (b) and a strain profile across the well (c). We measure an averaged In content (15±1%) in these InGaN QWs which is slightly smaller than the provided growth parameter (~17%) due to strain relaxation in the thin TEM foil (<5nm, see later discussion).

3.3 Single In atom detection

Considering an In concentration of 17% and a sample thickness of < 5nm close to the edge of the prepared HRTEM sample only 2-3 In atoms replace Ga atoms in each column on an average. This opens the perspective to try determining the In content column by column accounting for each single In atom. The high sensitivity of the OAM makes this task feasible.

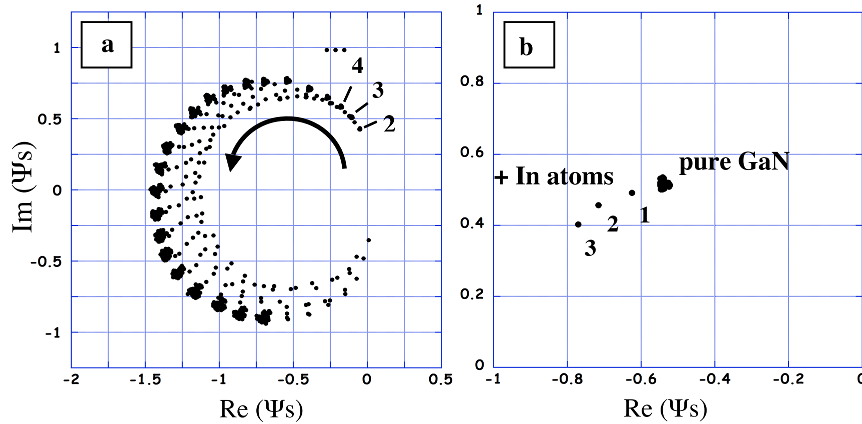

Figure 7: Data from multi slice simulations (300keV, debye waller = 0.5Å^{-1}): (a) Channeling map of Ψs of InGaN [11$\underline{2}$0] for thicknesses from 2, 3, 4, … up to 24 unit cells, single data points inside the "main circle" indicate the In atoms in the Ga column for each thickness; (b) zoom of (a) showing Ψs of InGaN for only one thickness with 1,2, and 3 In atoms in Ga column.

The channeling maps of Fig. 7 created by multi-slice calculations depict the principle of the approach. Figure 7a shows a channeling map of Ψs for InGaN and GaN where the sample thickness increases by atomic steps from 2 up to 24 unit cells (each atom is separated by 3.19Å in [11$\underline{2}$0] column direction). The amplitude of Ψs for pure GaN (data point clusters) shows a maximum at a thickness of about 16 unit cells (~50Å, left side of the circle) and the phase increases linearly by a characteristic phase change per atom. The single additional data points inside the GaN circle describe Ψs values if up to 7 In atoms reside in a Ga column. If the thickness of the specimen is constant, the exchange of a Ga atom by an In atom leads to a well defined phase change while amplitudes are hardly affected (Fig. 7b). The multi-slice simulations indicate a phase change per atom for Ga of about 0.161 rad and a phase change of an In atom that replaces a Ga atom of about 0.138 rad (~86% of a phase change per Ga atom). Simulated values depend on the chosen debye waller factor that describes the thermal vibration of the atoms and may cause discrepancies with the experiment. However, the ratio between the phase change per Ga atom (0.161 rad) and the phase change for an In atom at a Ga site (0.138 rad) can be extracted reliably (~86%).
Figure 8a shows amplitude and phase of Ψs of an InGaN QW (indicated by arrows) in a GaN matrix. A channeling map from regions of pure GaN is shown in Fig. 8b (marked in the amplitude image in Fig. 8a). The angular distribution of the data (Fig. 8c) reveals the detection of single atomic steps and a phase change per Ga atom of 0.145 rad. This experimental value is slightly smaller than the calculated one of 0.161 rad. The discrepancy is and attributed to our estimate of the debye waller factor in the simulations. Considering a ~14% smaller phase increment for an exchange of a Ga - by an In atom, a phase increment of ~0.125 rad should occur if indium substitutes for gallium.

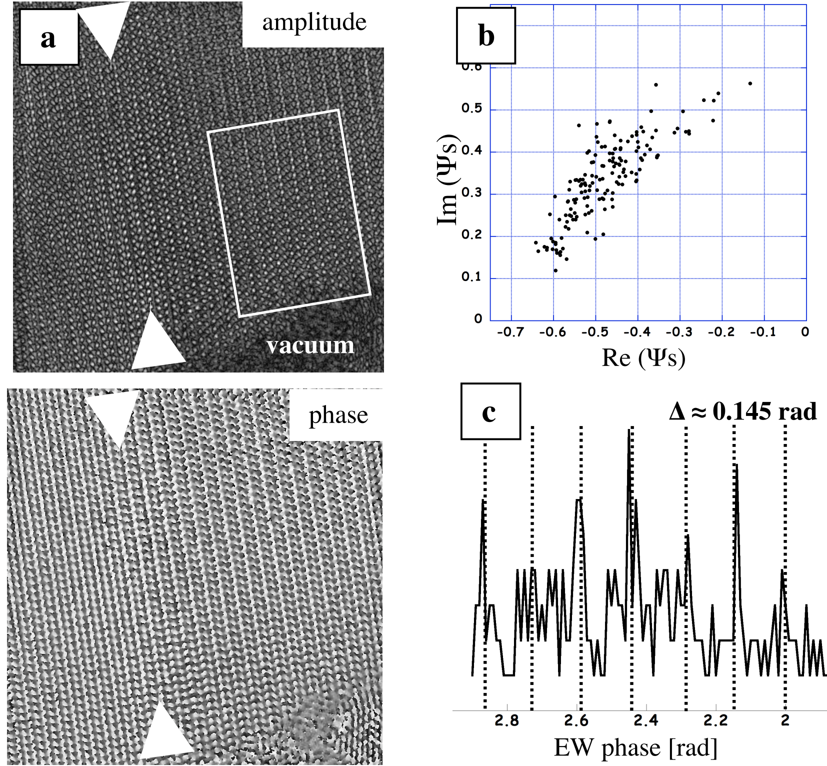

Figure 8: (a) Exit wave images (Ψs) of InGaN/GaN[11$\underline{2}$0], the InGaN QW is indicated by arrows; (b) Channeling map of data from the GaN region (marked in (a)) determining the phase sensitivity in this experiment; (c) angular distribution of the data in (b) showing a phase change per atomic step of Ga in GaN of about 0.145 rad.

The EW phase values extracted from Fig. 8a reveal a thickness gradient in this particular sample perpendicular to the sample edge as indicated by an arrow in Fig. 9a. We extract channeling maps for constant thickness in the GaN and assume that the thickness does not change in regions of InGaN. The considered regions are marked as area b and c in Fig. 9a. The GaN data in these two regions are 0.145 rad apart, which represents one atomic step in GaN. In both channeling maps from area b and c (Fig. 9b,c) a "green diamond" depicts the expected data point for pure GaN, and "red squares" show the data points for the substitution of 1, 2, 3 or 4 In atoms are in the Ga column. The angular data distribution is plotted in Fig. 9d together with our expectations of a 0.125 rad phase change per substituted In atom. We find satisfactory agreement.

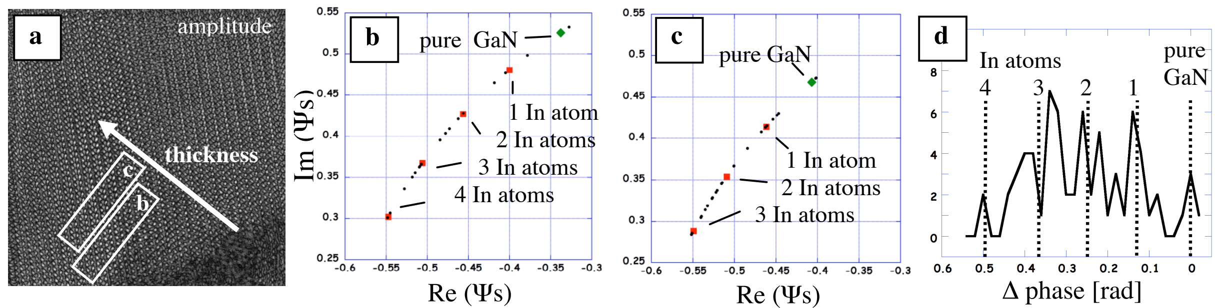

Figure 9: (a) Exit wave amplitude images Ψs of InGaN/GaN [11$\underline{2}$0], marked areas b and c which have uniform thickness (see arrow for thickness gradient); (b) Channeling map of EW values in InGaN region marked as "b" in (a), "green diamond" indicates expected data points of pure GaN, "red squares" indicate calculated data points of 1, 2, 3 or 4 In atoms in the Ga column at this thickness; (c) Channeling map of values of region marked as "c" in (a), area is exact 1 unit cell thicker than "b"; (d) shows the angular distribution of these data (GaN data are normalized to 0)

A further check of our approach can be performed by comparing the determined number of indium atoms with the data produced by strain measurements in Fig. 6. Figure 10a shows the relation of the analyzed atomic columns from area b (Fig. 9a,b) with the strain map in Fig. 6b. Following the indicated scan direction (arrow) we compare in the diagram in Fig. 10b the number of In atoms in each column ("blue diamonds") with the measured averaged c-axis strain (solid line). As mentioned above the lateral resolution of a strain map is about 0.5 nm and the width of an interface can be determined by fitting to an accuracy of about 0.1-0.4nm [2].

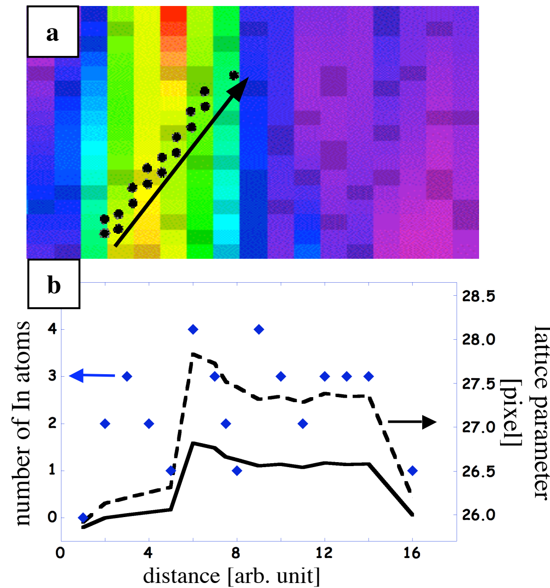

Figure 10: Comparison of data from strain measurements (Fig. 6b) with counted number of indium atoms from map in Fig. 9b; (a) indication of analyzed atomic columns (area b in Fig. 9a); (b) diagram showing number of In atoms ("blue diamonds") in each atomic column compared with measured relaxed strain (solid line) and evaluated non-relaxed strain (dashed line) – scan direction as indicated by arrow in (a).

Considering a thickness of this area of 10 unit cells (~32nm, extracted from the GaN analyses in Fig. 7 and 8) a strain relaxation in this thin TEM foil takes places. It results in an underestimation of the In concentration (~15%) using a strain map. If we correct for this relaxation by estimating the fully strained situation, that was calibrated with the local indium concentration ($\varepsilon_c/\varepsilon_a$ = - 0.54 … - 0.6 [29] - dashed line in diagram) we measure a local In content of ~22% which is 5 % higher than the average and nominal concentration 17%. It is satisfactory to find in Fig. 10b that the data points from our intensity measurement scatter around the strain estimation that accounts for a fully strained situation. The averaged In content per column of 2.31 atoms (37 atoms in 16 data point) and the thickness of 10 unit cells provides an In concentration of ~23%.

4 . CONCLUSIONS

Up to now the local indium (In) concentration and the degree of In segregation in an InGaN quantum well (QW) was determined by methods with limited resolution, e.g. by local strain analyses from single HRTEM images with a resolution of the size of the lattice parameters (0.5 nm x 0.3 nm). This paper proposes a new and general method using phase contrast microscopy to count single In atoms inside In_XGa_{1-X} columns of InGaN using sub Ångstrom resolution, a high S/N ratio (sensitivity) that results in a detection ability of light atoms (Z > 5-10).
In a gold [110] sample a suitable interpretation of exit wave (EW) amplitude and phase is established. Real and complex values of the channeling electron wave Ψs are considered. The amplitude is strongly peaked at the column positions while the phase is proportional to the column "weight": it increases linearly with thickness with a phase change per atom that is characteristic for the considered element. An easy way to display and interpret the EW values is the channeling map (an Argand plot). In case of gold a 3D thickness map is created.
Suitable InGaN/GaN specimen were prepared site specific with a focused ion beam (FIB) process followed by wet KOH etching. This preparation procedure results in unusual smooth sample surfaces. Multi-slice calculations along with

simulated EW images were used to validate our approach. We find that our sensitivity suffices to detect a single In atom in a column of Ga atoms.
Strain measurements from identical areas are suitable for checking this approach. Such analyses in the thin TEM specimen were performed revealing strain relaxation in the 5 nm thin foil. Compensating for the relaxation we find an average of 22% of indium from strain measurements that compares with 23% of indium content determined by our new method on an identical area of the sample.

ACKNOWLEDGEMENTS

This research was supported by the Laboratory Technology Research Division (SC-32), within the Office of Science, US Department of Energy under a CRADA (Cooperative Research and Development Agreement) between Lawrence Berkeley National Laboratory (LBNL) and Lumileds Lighting, San Jose/CA under US DOE Contract DE-AC03-76SF00098. J.R. Jinschek was supported by a Feodor-Lynen-Fellowship of the Alexander von Humboldt-Foundation, Bonn/Germany (http://www.avh.de).

REFERENCES

1. S. Nakamura, T. Mukai, M. Senoh, S. Nagahama, and N. Iwasa, "$In_xGa_{(1-x)}N/In_yGa_{(1-y)}N$ superlattices grown on GaN films", *J. Appl. Phys.*, **74**, 3911-3915, 1993.
2. Ch. Kisielowski, Z. Liliental-Weber, S. Nakamura, "Atomic Scale Indium Distribution in a GaN / $In_{0.43}Ga_{0.57}N$ / $Al_{0.1}Ga_{0.9}N$ Quantum Well Structure", *Jpn. J. Appl. Phys. (Part 1)*, **36**, 6932-6936, 1997.
3. D. Gerthsen, E. Hahn, B. Neubauer, A. Rosenauer, O. Schön, M. Heuken, A. Rizzi, "Composition Fluctuations in InGaN Analyzed by Transmission Electron Microscopy", *phys. stat. sol. (a)*, **177**, 145-155, 2000.
4. C. Kisielowski, "Composition and Strain Fluctuations in InN/GaN/AlN Heterostructures", *Proceedings 2nd International Symposium on Blue Laser and Light Emitting Diodes*, Chiba Japan, Ohmsha Ltd, 321-326, 1998.
5. K. Watanabe, J.-R. Yang, N. Nakanishi, K. Inoke, M. Shiojiri, "Direct determination of atomic structure in multiple quantum wells InGaN/GaN", *Appl. Phy. Lett.*, **80**, 761-762, 2002.
6. D. Van Dyck, M. Op de Beeck, W. Coene, "A new appraoch to object wavefunction reconstruction in electron microscope", *Optik: Zeitschrift für Licht- und Elektronenoptik*, **93**:3, 103-107, 1993.
7. H. Lichte, "Electron image plane off-axis holography of atomic structures", in *Advances in Optical and Electron Microscopy*, Eds. T. Mulvey and C. Sheppard, Vol. 12, 25-91, Academic Press, London, 1991.
8. C. Kisielowski, C.J.D. Hetherington, Y.C. Wang, R. Kilaas, M.A. O'Keefe, A. Thust, "Imaging columns of the light elements carbon, nitrogen and oxygen with sub Angstrom resolution", *Ultramicroscopy*, **89**, 243-263, 2001.
9. J. Ayache, P. H. Albarède, "Application of the ionless tripod polisher to the preparation of YBCO superconducting multilayer and bulk ceramics thin films", Ultramicroscopy **60**, 195-206, 1995.
10. G.A. Botton, M.W. Phaneuf, "Imaging, spectroscopy and spectroscopic imaging with an energy filtered field emission TEM", *Micron*, **30**, 109-119, 1999.
11. W.M.J. Coene, A. Thust, M. Op de Beeck, D. Van Dyck, "Maximum-likelihood method for focus-variation image reconstruction in high resolution transmission electron microscopy", *Ultramicroscopy*, **64**, 109-135, 1996.
12. A. Thust, W.M.J. Coene, M. Op de Beeck, D. Van Dyck, "Focal-series reconstruction in HRTEM: simulation studies on non-periodic objects", *Ultramicroscopy*, **64**, 211-230, 1996.
13. J.R. Jinschek, C. Kisielowski, M. Lentzen, K. Urban, "Quantification of the Resolved Phase Change in Reconstructed Electron Exit Waves of Gold [110] in Different Electron Microscopes", *Microsc. Microanal.*, **8** (Suppl. 2), 466-467CD, 2002.
14. A. Thust, M.H.F. Overwijk, W.M.J. Coene, M. Lentzen, "Numerical correction of lens aberrations in phase-retrieval HRTEM", *Ultramicroscopy*, **64**, 249-264, 1996.
15. M.A. O'Keefe, C.J.D. Hetherington, Y.C. Wang, E.C. Nelson, J.H. Turner, C. Kisielowski, J.-O. Malm, R. Mueller, J. Ringnalda, M. Pam, A. Thust, "Sub-Ångstrom high-resolution transmission electron microscopy at 300"keV", *Ultramicroscopy*, **89**, 215-241, 2001.
16. D. van Dyck, J.H. Chen, "A simple theory for dynamical electron diffraction in crystals", *Solid State Communications*, **109**, 501-505, 1999.
17. S.J. Pennycook, B. Rafferty, P.D. Nellist, "Z-contrast imaging in an aberration-corrected scanning transmission electron microscopy", *Microsc. Microanal.*, **6**, 343-352, 2000.

18. Ch. Kisielowski, J.R. Jinschek, “On the Feasibility to Investigate Point Defects by Advanced Electron Microscopy”, *Physics of Microstructured Semiconductors*, **27**, 137-144, 2002.
19. P. M. Voyles, D. A. Muller, J. L. Grazul, P. H. Citrin, H.-J. L. Gossmann, “Atomic-scale imaging of individual dopant atoms and clusters in highly n-type bulk Si”, *Nature*, **416**, 826-829, 2002.
20. P. M. Voyles, J. L. Grazul, D. A. Muller, “Imaging individual atoms inside crystals with ADF-STEM”, *Ultramicroscopy*, **96**, 251–273, 2003.
21. T. Radetic, U. Dahmen, “Influence of Germanium Interdiffusion on the Morphological Evolution of Σ3 Grain boundaries in Gold Thin Films”, *Microsc. Microanal.*, **8** (Suppl. 2), 1404-1405CD, 2002.
22. D. Van Dyck, M. Op De Beeck, “A simple intuitive theory for electron diffraction”, *Ultramicroscopy*, **64**, 99-107, 1996.
23. P. Geuens, D. Van Dyck, “The S-state model: a work horse for HRTEM”, *Ultramicroscopy* **93**, 179–198, 2002.
24. D. Van Dyck, P. Geuens, J. R. Jinschek, C. Kisielowski, “From exit wave to atomic structure”, *Proceedings International Workshop on Noncrystallographic Phase Retrieval*, Cairns (Australia), will be published, 2003.
25. W. Sinkler, L.D. Marks, “Dynamical direct methods for everyone”, *Ultramicroscopy*, **75**, 251-268, 1999.
26. J.R. Jinschek, Ch. Kisielowski, P. Geuens, D. Van Dyke, will be published, 2003.
27. M.V. Moore, “Recent advances in DB TEM sample preparation”, *Microsc. Microanal.*, **8** (Suppl. 2), 60-61, 2002.
28. J.R. Jinschek, Ch. Kisielowski, will be published, 2003.
29. C. Kisielowski, J. Krueger, S. Ruvimov, T. Suski, J.W. Ager III, E. Jones, Z. Lilienthal-Weber, M. Rubin, E.R. Weber, M.D. Bremser, R.F. Davis, “Strain-related phenomena in Gan thin films”, *Physical Review B*, **54**, 17745-17753, 1996.